Supporting Information

Modulating discharge capacity and cycling performance of $LiMn_{0.6}Fe_{0.4}PO_4$ cathode for lithium-ion batteries via titanium introduction

Jing Han [a,b,*], Weiling Jiang [a,c], Qihang Wang [b], Huichao Lu [b], Weiqin Wang [b], Shiqiang Luo [b,*]

[a]College of New Energy, Xi'an Shiyou University, Xi'an, Shaanxi 710065, P. R. China;

[b]Shanghai Electrochemical Energy Devices Research Center, School of Chemistry and Chemical Engineering, Shanghai Jiao Tong University, Shanghai 200240, P. R. China;

[c]Key Laboratory of Synthetic and Natural Functional Molecule Chemistry of the Ministry of Education, Xi'an Key Laboratory of Functional Supramolecular Structure and Materials, College of Chemistry and Materials Science, Northwest University, Xi'an 710127, P. R. China

* Corresponding author: E-mail addresses: jinghan@xsyu.edu.cn (J. Han), ltlsqiang@sjtu.edu.cn (S. Luo).

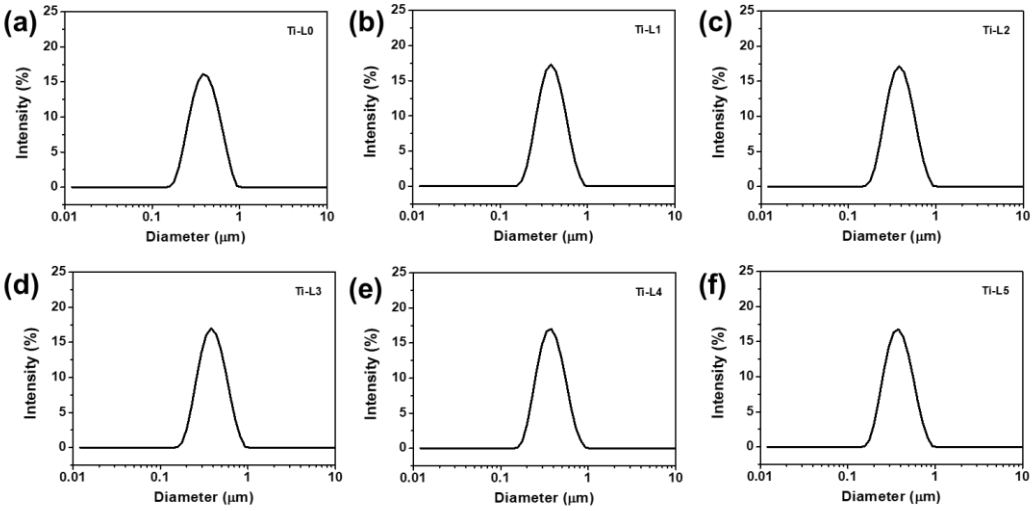

Figure S1 Particle size distribution curves of (a) Ti-L0, (b) Ti-L1, (c) Ti-L2, (d) Ti-L3, (e) Ti-L4, (f) Ti-L5 after ball-milling during preparation.

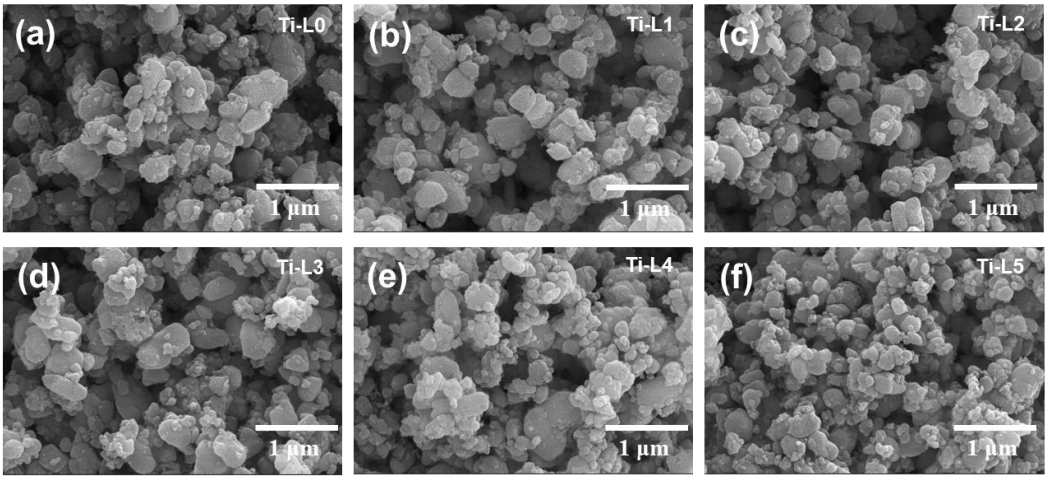

Figure S2 SEM images of (a) Ti-L0, (b) Ti-L1, (c) Ti-L2, (d) Ti-L3, (e) Ti-L4, (f) Ti-L5.

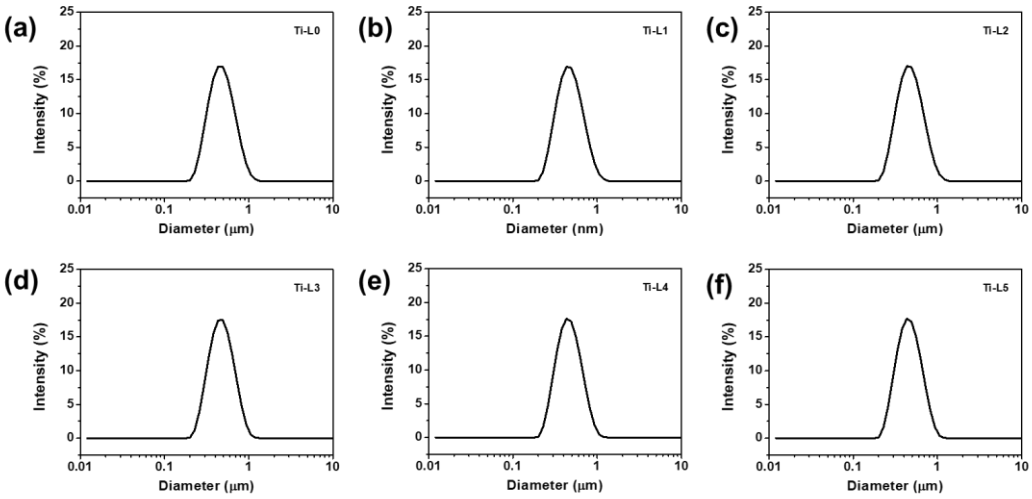

Figure S3 Particle size distribution curves of (a) Ti-L0, (b) Ti-L1, (c) Ti-L2, (d) Ti-L3, (e) Ti-L4, (f) Ti-L5.

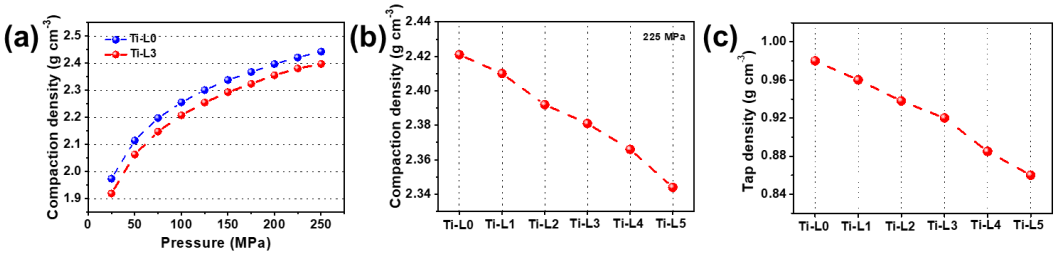

Figure S4 (a) Compaction density distribution at different pressures of Ti-L0 and Ti-L3. (b) Compaction density and (c) tap density of Ti-L0, Ti-L1, Ti-L2, Ti-L3, Ti-L4, Ti-L5.

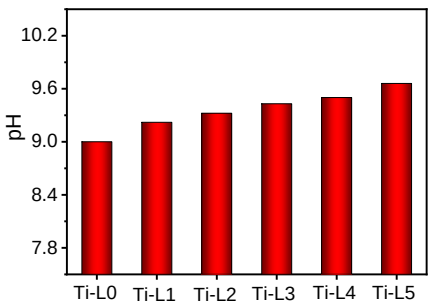

Figure S5 pH values of Ti-L0, Ti-L1, Ti-L2, Ti-L3, Ti-L4, Ti-L5.

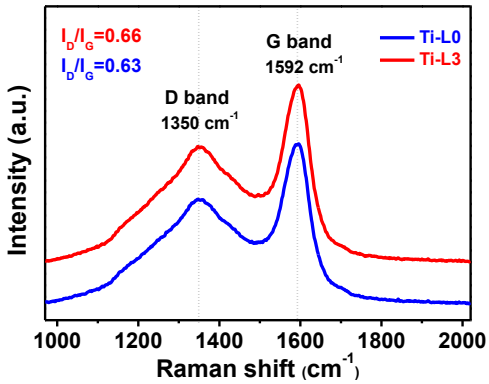

Figure S6 Raman spectra of Ti-L0 and Ti-L3.

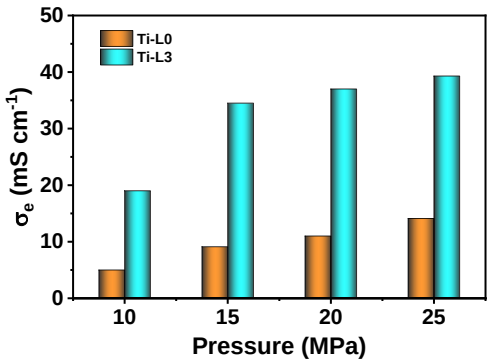

Figure S7 Electronic conductivities at different pressures of Ti-L0 and Ti-L3.

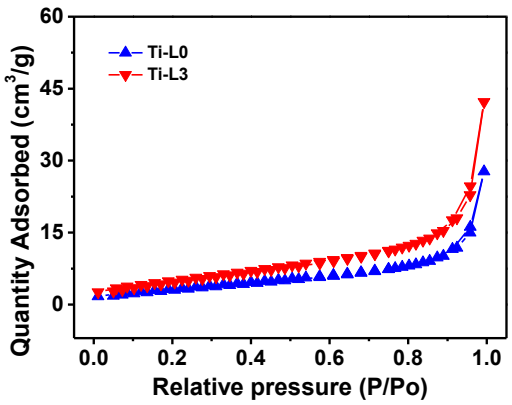

Figure S8 N_2 adsorption−desorption isotherm curves of Ti-L0 and Ti-L3.

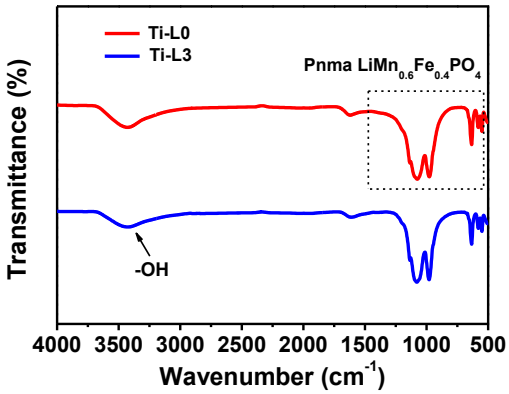

Figure S9 FT-IR spectra of Ti-L0 and Ti-L3.

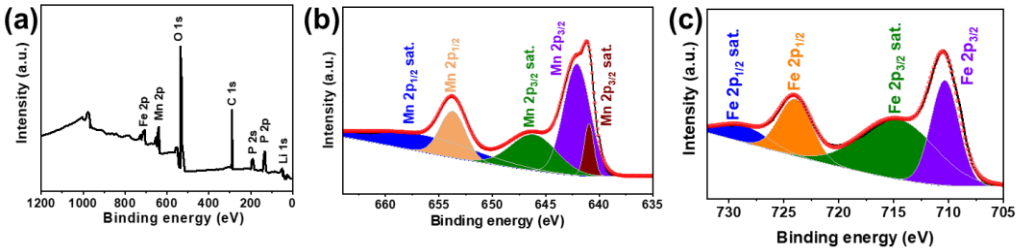

Figure S10 (a) XPS full spectra, (b) Mn 2p, (c) Fe 2p spectra of Ti-L0

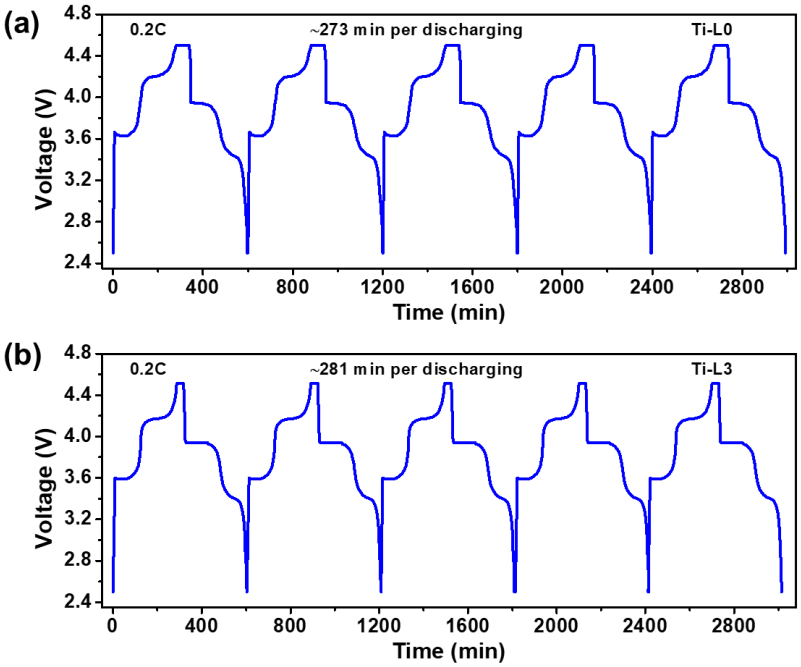

Figure S11 Time-voltage profiles of (a) Ti-L0 and (b) Ti-L3 at 0.2 C.

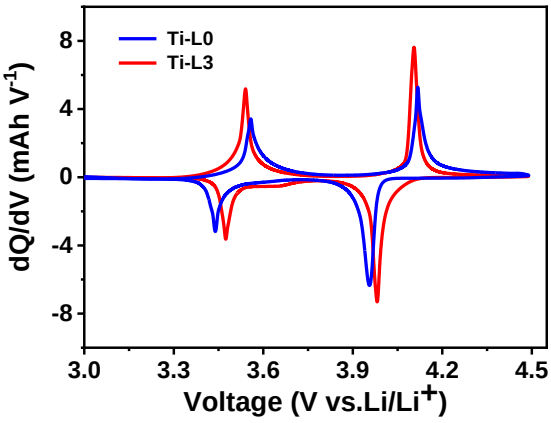

Figure S12 Differential capacities as a function of voltage for Ti-L0 and Ti-L3.

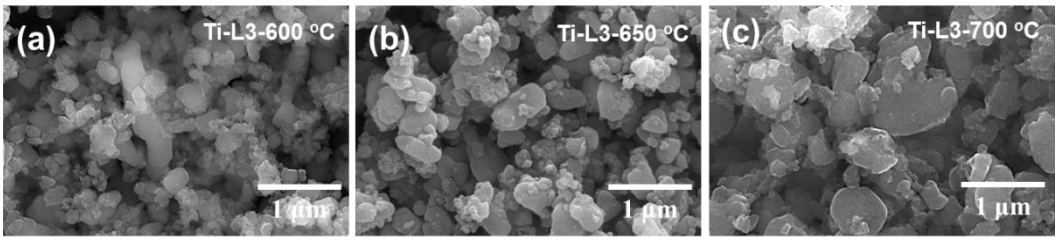

Figure S13 SEM images of Ti-L3 prepared at (a) 600 °C, (b) 650 °C, (c) 700 °C

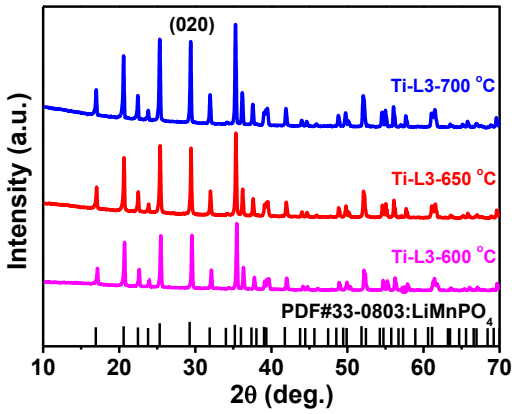

Figure S14 XRD of Ti-L3 prepared at 600 °C, 650 °C, 700 °C.

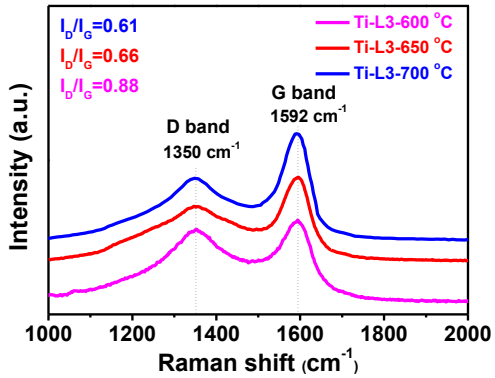

Figure S15 Raman spectra of Ti-L3 prepared at 600 °C, 650 °C, 700 °C.

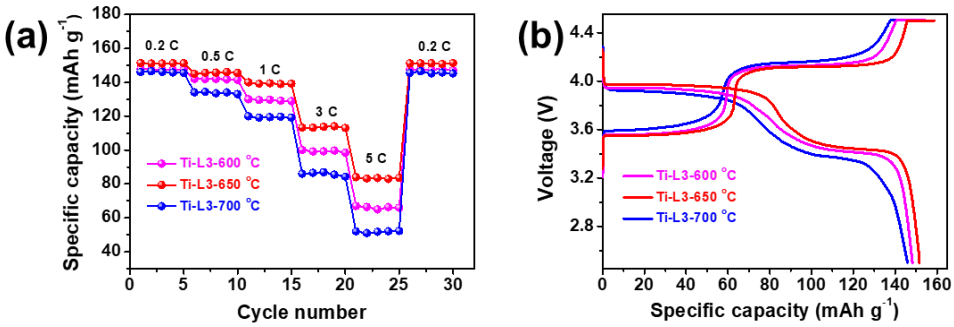

Figure S16 (a) Rate performance and (b) discharge profiles at 0.2 C of Ti-L3 prepared at 600 °C, 650 °C, 700 °C.

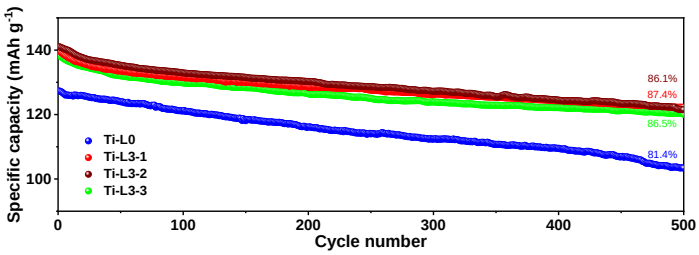

Figure S17 Cycling performance at 1 C at room temperature of Ti-L0 and three Ti-L3 samples.

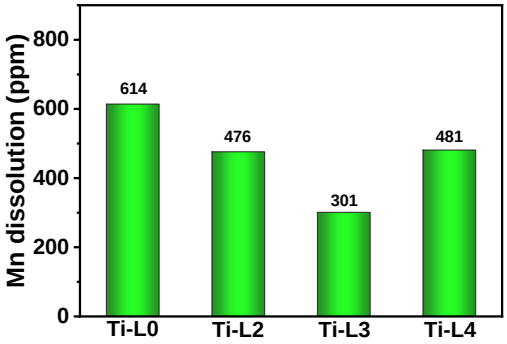

Figure S18 Content of Mn deposited on negative electrode after 500 cycles based on ICP.

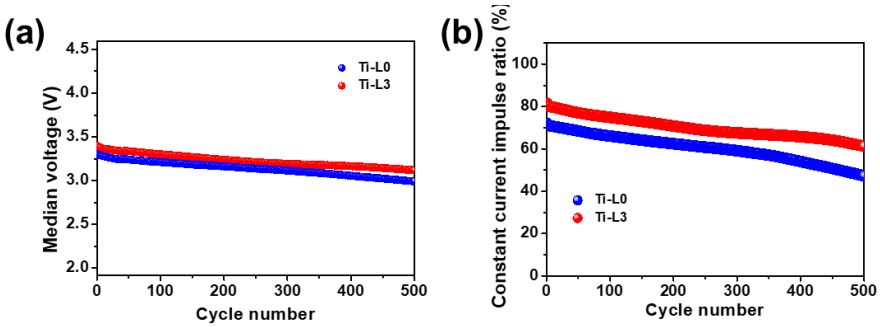

Figure S19 (a) Median voltage and (b) constant current impulse ratio of Ti-L0 and Ti-L3 during cycling at 1 C.

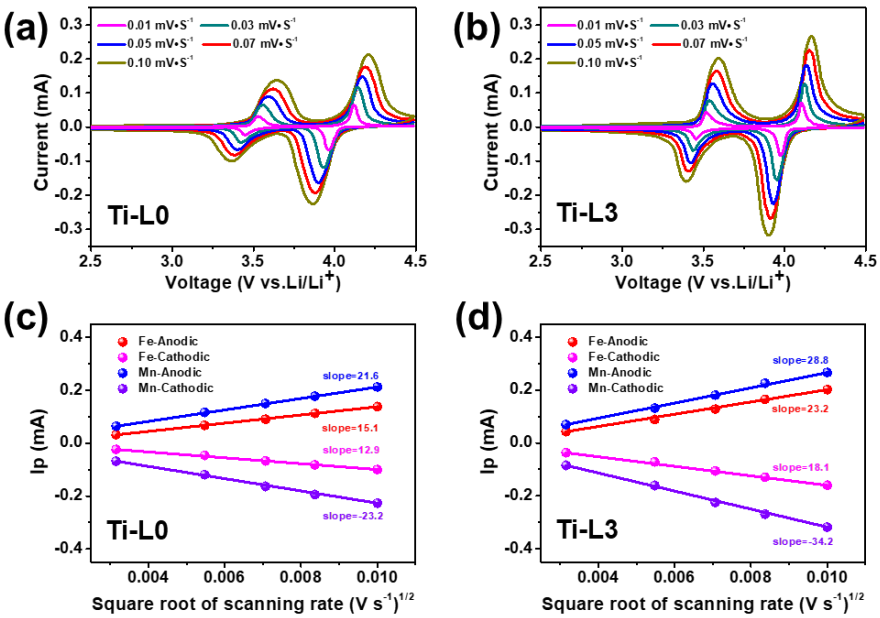

Figure S20 CV curves of (a) Ti-L0 and (b) Ti-L3 at the scanning rate of 0.01-0.01 mV s^{-1}, The corresponding relationships between I_p and $\upsilon^{1/2}$ of (c) Ti-L0 and (d) Ti-L3.

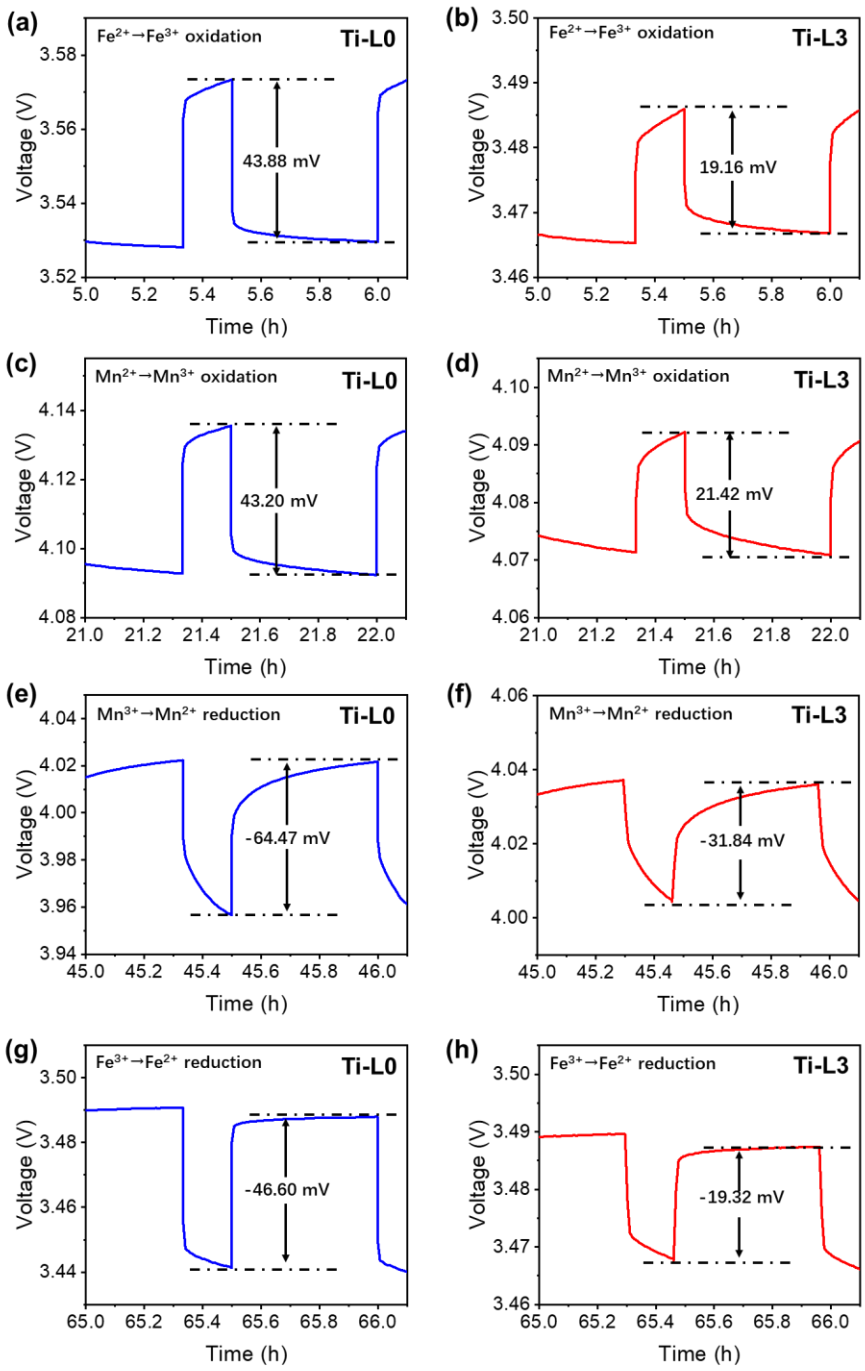

Figure S21 Titration fragments of (a, c, e, g) Ti-L0 and (b, d, f, h) Ti-L3 samples during Fe^{2+}/Fe^{3+} and Mn^{2+}/Mn^{3+} redox reaction. The current pulse time is 600 s and rest time is 1800 s.

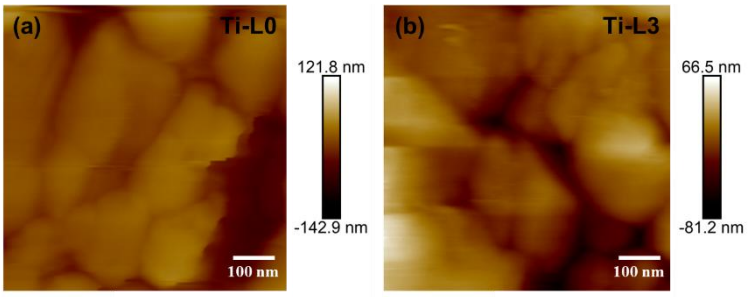

Figure S22 AFM height images (2D) of (a) Ti-L0 and (b) Ti-L3.

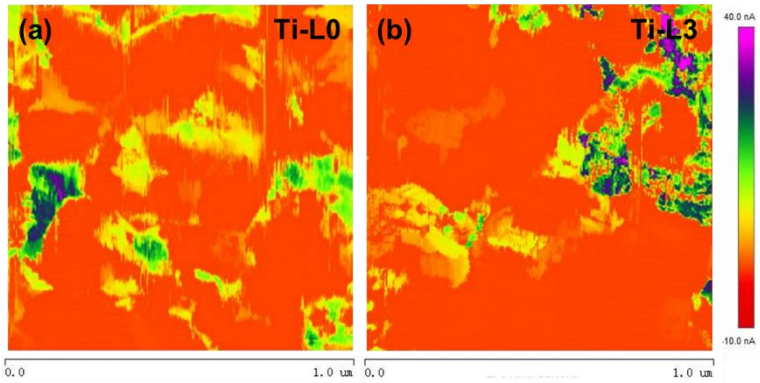

Figure S23 Current maps (2D) of (a) Ti-L0 and (b) Ti-L3 by C-AFM.

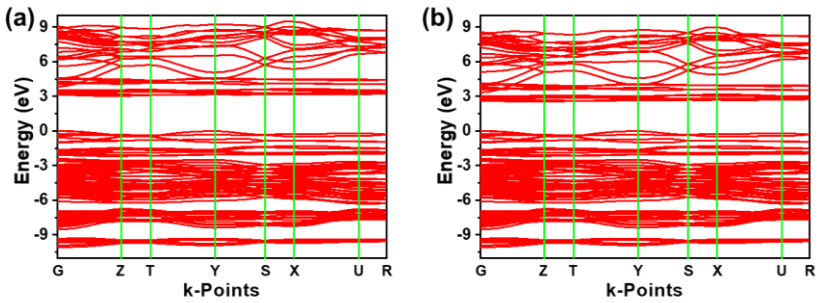

Figure S24 Energy band structure of (a) Ti-L0 and (b) Ti-L3 based on DFT calculation.

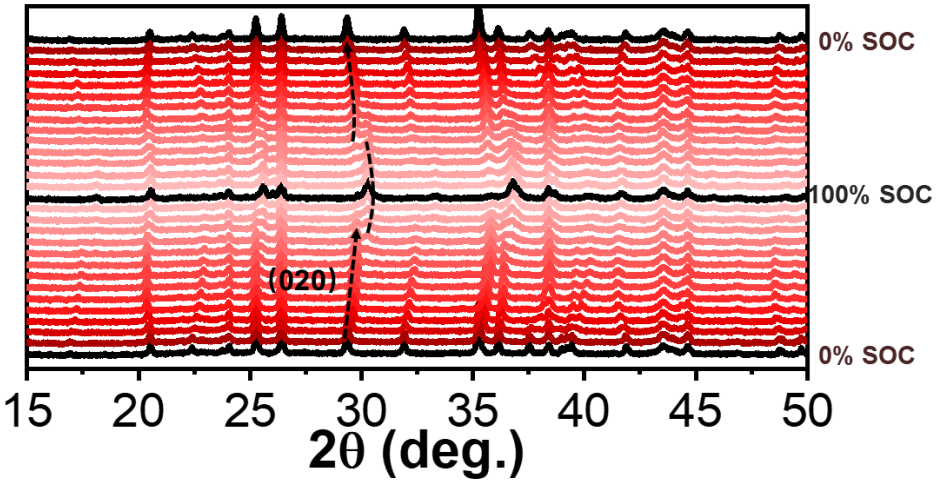

Figure S25 The waterfall profiles of in situ XRD patterns during the charge/discharge process at 0.2 C for Ti-L0 sample.

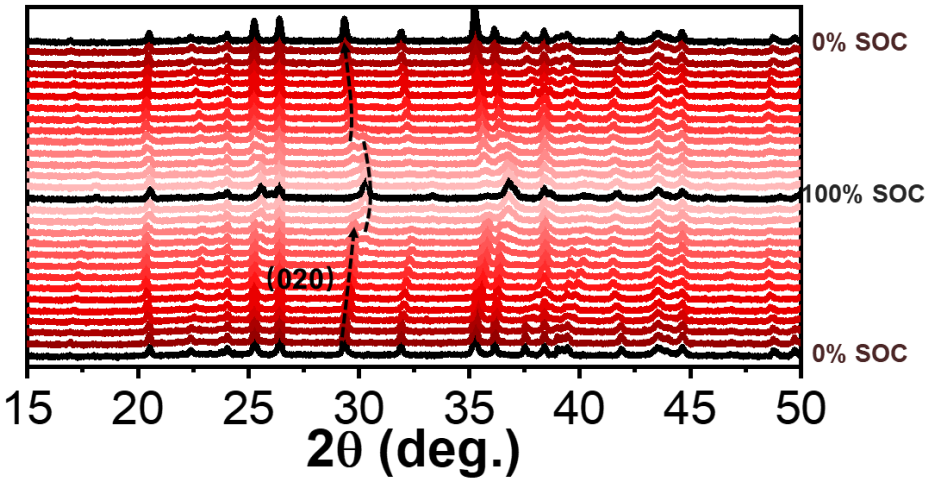

Figure S26 The waterfall profiles of in situ XRD patterns during the charge/discharge process at 0.2 C for Ti-L3 sample.

Table S1 Structural parameters of Ti-L0 and Ti-L3 from the Rietveld refinement of XRD patterns

	a (Å)	b (Å)	c (Å)	V (Å^3)
Ti-L0	10.401	6.062	4.721	297.663
Ti-L3	10.395	6.059	4.719	297.218

Table S2 The atom positions in the Ti-L0 crystal structure.

	X	Y	Z	Occupancy
Li1	0.00000	0.00000	0.00000	1
Mn1	0.28278	0.25000	0.97078	0.6
Fe1	0.28278	0.25000	0.97078	0.4
P1	0.09488	0.25000	0.41634	1
O1	0.09586	0.25000	0.73048	1
O2	0.45138	0.25000	0.20564	1
O3	0.16024	0.05282	0.27857	1

Table S3 The atom positions in the Ti-L3 crystal structure.

	X	Y	Z	Occupancy
Li1	0.00000	0.00000	0.00000	1
Mn1	0.28262	0.25000	0.97107	0.57
Fe1	0.28262	0.25000	0.97107	0.4
Ti1	0.28262	0.25000	0.97107	0.03
P1	0.09488	0.25000	0.41634	1
O1	0.09578	0.25000	0.73205	1
O2	0.45014	0.25000	0.21444	1
O3	0.16012	0.05271	0.27865	1

Table S4 The length of Li-O1, Li-O2 and Li-O3 for Ti-L0 and Ti-L3 samples from the Rietveld refinement of XRD patterns

	Li-O1(Å)	Li-O2 (Å)	Li-O3(Å)
Ti-L0	2.2158	2.0952	2.1512
Ti-L3	2.2204	2.1223	2.1520

Table S5 Particle size parameters of all samples.

	D10(μm)	D50 (μm)	D90(μm)
Ti-L0	0.337	0.461	0.891
Ti-L1	0.321	0.452	0.805
Ti-L2	0.320	0.449	0.767
Ti-L3	0.315	0.441	0.748
Ti-L4	0.306	0.427	0.721
Ti-L3	0.299	0.405	0.693

Table S6 Physical parameters of all samples

Sample	Carbon content (wt.%)	Compaction density (g cm^{-3})	pH	Electronic conductivity (μS cm^{-1})	Specific surface area (m^2 g^{-1})
Ti-L0	1.81	2.42	9.01	0.011	18.23
Ti-L1	1.76	2.41	9.22	0.032	20.18
Ti-L2	1.85	2.39	9.32	0.031	20.76
Ti-L3	1.79	2.38	9.43	0.037	21.39
Ti-L4	1.71	2.36	9.51	0.030	22.47
Ti-L5	1.82	2.34	9.66	0.033	23.51

Table S7 Comparisons of performances and preparation method between this work and the previously reported $LiMn_{0.6}Fe_{0.4}PO_4$ material.

Materials	Specific capacity (mAh g^{-1})	Cycle performance	Preparation method	Ref.
$LiMn_{0.6}Fe_{0.4}PO_4$/NC	156.8 at 0.1 C, 122.2 at 1 C	94.6 % after 200 cycles at 1 C	Solvothermal method	1
$LiMn_{0.8}Fe_{0.2}PO_4$/C	161 at 0.2 C, 105 at 1 C	76.4 % after 30 cycles at 0.2 C	Solid state method	2
$0.9LiMn_{0.7}Fe_{0.3}PO_4 \cdot 0.1Li_3V_2(PO_4)_3$	154.6 at 0.5 C, 90.9 at 50 C	98% after 200 cycles at 0.5 C	Solvothermal method	3, 4
$LiMn_{0.7}Fe_{0.3}PO_4$/C	149.1 at 0.1 C, 110.6 at 1 C	96.1% after 160 cycles at 0.1 C	Solid state method	5
$LiMn_{0.6}Fe_{0.4}PO_4$/C-F/G	155.4 at 0.2 C, 130.1 at 1 C	85.8% after 100 cycles at 0.1 C	Solvothermal method	6
$LiMn_{0.6}Fe_{0.4}PO_4$-SP-HCN	150.4 at 0.2 C, 133.7 at 1 C	86.3% after 500 cycles at 1 C,	Solid state method	7
$LiMn_{0.25}Mg_{0.05}Fe_{0.7}PO_4$/C	155.2 at 0.2 C, 142.0 at 1 C	98.6% after 50 cycles at 0.1 C	Solid state method	8
$LiMn_{0.6}Fe_{0.4}PO_4$/C	153.8 at 0.1C, ~128 at 1 C	98.5% after 50 cycles at 0.1 C	Spray drying method	9
$LiMn_{0.6}Fe_{0.25}Mo_{0.15}PO_4$/C	153.2 at 0.2 C, ~132 at 1 C	91.4% after 100 cycles at 1 C	Solid state method	10
$LiMn_{0.6}Fe_{0.4}PO_4/C/Al_2O_3$	131.4 at 0.2 C, 111.2 at 1 C	99.3% after 500 cycles at 1 C	Solvothermal method	11
$LiMn_{0.5}Fe_{0.49}Zn_{0.01}PO_4$/C	148.9 at 0.1 C, 128.8 at 1 C	92.6 % after 100 cycles at 2 C	Solvothermal method	12
$LiMn_{0.6}Fe_{0.25}Nb_{0.15}PO_4$/C	156.7 at 0.2 C, 134.5 at 1 C	95.6% after 100 cycles at 1 C	Solid state method	13
$LiMn_{0.6}Fe_{0.395}La_{0.005}PO_4$/C	153.0 at 0.2 C, 138.3 at 1 C	96.5 after 600 cycles at 1 C	Solid state method	14
$LiMn_{0.57}Ti_{0.03}Fe_{0.4}PO_4$/C	151.4 at 0.2 C, 139.3 at 1 C	87.4% after 500 cycles at 1 C	Solid state method	This work

Table S8 Cost structure of lithium manganese iron phosphate ($LiMn_{0.6}Fe_{0.4}PO_4$) production.

Item	Raw material	Unit price (¥/ton)	Consumption (ton)	Unit cost (¥/ton)	Cost (¥/ton)
Material cost	$FePO_4$	12000	0.39	4680	30995
	Li_2CO_3	65000	0.1	6500	
	Mn_3O_4	17000	0.29	4930	
	LiH_2PO_4	35000	0.4	14000	
	glucose	12000	0.005	60	
	PEG	20000	0.03	600	
	TiO_2	4500	0.05	225	
Energy cost					5000
Labor cost					400
Total cost					**36395**

Table S9 The kinetic simulation results based on EIS.

Sample	R_{ct} (Ω)	D_{Li+} ($cm^2\ s^{-1}$)
Ti-L0	176.2	3.78×10^{-14}
Ti-L1	146.5	9.62×10^{-14}
Ti-L2	126.3	2.06×10^{-13}
Ti-L3	112.6	5.60×10^{-13}
Ti-L4	127.1	3.31×10^{-13}
Ti-L5	148.7	8.02×10^{-14}

Table S10 Li^+ diffusion coefficients (D_{Li+}) of Ti-L0 and Ti-L3 based on CV.

Sample	D_{Li+}-Fe anodic ($cm^2\ s^{-1}$)	D_{Li+}-Fe cathodic ($cm^2\ s^{-1}$)	D_{Li+}-Mn anodic ($cm^2\ s^{-1}$)	D_{Li+}-Mn cathodic ($cm^2\ s^{-1}$)
Ti-L0	4.74×10^{-12}	3.46×10^{-12}	9.69×10^{-12}	1.12×10^{-11}
Ti-L3	1.12×10^{-11}	6.81×10^{-12}	1.72×10^{-11}	2.43×10^{-11}

References

1. J. Zhang, Y. Liu, B. Wang and W. Yao, *Batteries Supercaps*, 2024, e202400105..
2. X. Yao, D. Li, L. Guo, M. Kallel, S. D. Alahmari, J. Ren, I. Seok, G. Roymahapatra and C. Wang, *Adv. Compos. Hybrid Ma.*, 2024, **7**, 63.
3. Q. Hu, J. Liao, X. Xiao, X. Wang, J. Liu, Y. Song, D. Ren, H. Zhang, L. Wang, Z. Chen and X. He, *Nano Energy*, 2022, **104**, 107895.
4. Q. Hu, L. Wang, G. Han, J. Liao, J. Liu, J. Yao and X. He, *Nano Energy*, 2024, **123**, 109422.
5. Y. Wang, Y. Deng, Y. Liu, X. Sun, Y. Wang, H. Liu, H. Zhou and P. He, *Energy Fuels*, 2024, **38**, 12265-12273.
6. M. Tan, H. Wei, Q. Li, Z. Yu, Q. Zhang, M. Lin and B. Lin, *Batteries*, 2024, **10**, 272.
7. M. Zhao, Y. Zhou, Y. Chen, X. Liang, K. Bai, J. Zeng and H. He, *Electrochim. Acta*, 2025, **521**, 145844.
8. K. Xia, R. Liang, Y. Luo, A. Zheng, G. Jiang, M. Fan, J. Xiong and S. Yuan, *Int. J. Electrochem. Sc.*, 2022, **17**, 221273.
9. S. Huang, W. Lin, L. Li, P. Liu, T. Huang, Z. Huang, J. kong, W. Xiong, W. Yu, S. Ye, J. Hu, Q. Zhang and J. Liu, *Prog. Nat. Sci.*, 2023, **33**, 126-131.
10. L. Wen, Z. Guan, L. Wang, X. Liu, G. Wen, Y. Zhao, D. Pang and R. Dou, *J. Mater. Eng. Perform.*, 2024, **33**, 12884–12890.
11. C. Li, X. Yu, C. Liao, Z. Cui, J. Zhu, M. Gao, W. Wang, F. Weng, R. Zou and Q. Liu, *ChemNanoMat*, 2024, **10**, e202300558.
12. B. J. Jeong, J. Y. Sung, F. Jiang, S. P. Jung and C. W. Lee, *J. Energy Storage*, 2024, **96**, 112552.
13. H. Guo, R. Liu, W. Li, H. Gu, J. Cao, D. Gong and G. Liang, *J. Electrochem. Soc.*, 2023, **170**.
14. J. Yu, J. Ma, H. Zhang, J. Hang, W. Tian, X. Tian and H. Yang, *Ceram. Int.*, 2025.